J. Earth Syst. Sci. (2020)129 50
https://doi.org/10.1007/s12040-019-1317-0

Implication of submarine groundwater discharge to coastal ecology of the Bay of Bengal

Kousik Das[1,*], Palash Debnath[2], Srimanti Duttagupta[1], Sukanta Sarkar[2], Sudha Agrahari[2] and Abhijit Mukherjee[1,2,3]

[1]*School of Environmental Science and Engineering, Indian Institute of Technology Kharagpur, Kharagpur, West Bengal, India.*
[2]*Geology and Geophysics, Indian Institute of Technology Kharagpur, Kharagpur, West Bengal, India.*
[3]*Applied Policy Advisory to Hydrogeosciences Group, Indian Institute of Technology Kharagpur, Kharagpur, West Bengal, India.*
**Corresponding author. e-mail: kousik.envs@gmail.com*

MS received 2 August 2019; revised 8 November 2019; accepted 14 November 2019

The present study is undertaken in the eastern coast of India, along the coastal tract of Bay of Bengal (BoB), to delineate the submarine groundwater discharge (SGD)-borne nutrient flux at temporal scale and their impact to coastal ecology and biogeochemical processes. Solutes chemistry, seepage meter study, stable-isotopic signature, and geophysical techniques were used to identify the surface water–groundwater interaction zone, SGD rate and nutrient flux. The estimated rate of major annual discharge of nutrient fluxes were 240 and 224 mM m^{-2} day^{-1} for NO_3^- and Fe_{tot}. The variation of solute and nutrient fluxes was depending on the load of terrestrial water masses, which is triggered by the local monsoonal meteoric recharge. The ecohydrological response to this solute flux results in spatio-temporal patterns of N and P-sensitive algal blooms in the intertidal zones. Most algae were identified as dinoflagellates and some haptophytes, with greenish and brownish hue that provides a distinct look to the coastal landscape. The algal blooms were found to be substantially influenced by the seasonal-nutrients flux and discharge location. Our study is expected to increase the understanding of a rarely reported eco-hydrological response to terrestrial–marine water interactions and their implications in the tropical ocean adjoining the Indian Subcontinent.

Keywords. SGD; Bay of Bengal; nutrient dynamics; solute transport; geochemical cycle; coastal hydrology.

1. Introduction

Two largest water masses, *viz.*, groundwater and seawater are interacting in coastal areas, where submarine groundwater discharge (SGD) was identified as a leading process in this seawater–groundwater (SW–GW) interaction zone for shallow depths. SGD was delineated as an essential source of transportation of nutrients/solutes, contaminants including trace elements to the marine ecosystem, which is largely influenced by local to regional hydrogeological cycles (Tamborski *et al.* 2017). During the transportation process SGD derived original chemical and/or isotopic composition of solutes/nutrients gets altered through the discharge path even in temporal to seasonal scale (Slomp and van Cappellen 2004; Debnath *et al.* 2018, 2019).

Published online: 09 January 2020

The understanding of the process controlling these dynamics and impacts of SGD derived nutrients, solutes and contaminants on its discharge path are inadequate in this SW–GW interaction study (Michael *et al.* 2005). SGD derived micro- (Mn, Fe) and macro- (NO_3^-, PO_4^{3-}) solute/nutrient flux plays a major contribution to budgeting of chemical constituents to global ocean (Roy *et al.* 2010). SGD contributed dissolved solutes/nutrients to coastal ecosystems may often have harmful effects on coastal ecosystem (Johannes 1980; Zektser *et al.* 2006; Beck *et al.* 2015). SGD derived nutrient flux may cause eutrophication leading to growth of algal blooms (Simmons 1992; Valiela *et al.* 2002; Hwang *et al.* 2005; Null *et al.* 2012).

SGD can vary spatially (depending on subsurface hydraulic properties and heterogeneity), as well as temporally (on a lunar tidal scale to seasonal scale (Rapaglia 2006; Gonneea *et al.* 2008)). Process behind the nutrients input through terrestrially derived-SGD (T-SGD) to the marine ecosystem is essential to understand as it acts as essential nutrient substrate for the littoral to neritic life-forms (Miller and Ullman 2004; Rocha *et al.* 2015).

However, the spatial and temporal complexities due to heterogeneous aquifer system make SGD associated quantification more difficult, therefore natural tracers are gradually being used in present advanced stage of global SGD studies. The application of natural traces like $\delta^{18}O$ coupled with the geochemical composition has lead to better understanding of the SW–GW interaction processes (Das and Mukherjee 2019; Debnath *et al.* 2019). As SGD varies spatially on a scale of few meters to kilometers and temporally, application of geophysical techniques like electrical resistivity tomography (ERT) have become common in the field of SW–GW studies (Zarroca *et al.* 2014). On the recent development of geophysical methods, electrical resistivity surveying, two-dimensional (2-D) electrical imaging surveys are extensively being used to project the variation in resistivity of aquifer both vertically and laterally in saline/freshwater saturated/unsaturated systems.

The present study was conducted at micro-tidal coast of Chandipur, Orissa, India, adjoining the Bay of Bengal (BoB), to delineate the SGD-derived nutrient/solute flux and its impact on coastal ecology. Solute chemistry, seepage meter study, stable-isotopic signature and ERT were used to identify the SGD rate and its spatial-to-depth dependent and temporal variability. Along with the field sampling and analysis, abundantly available algal species at the focused discharge point has also been identified. The study results may provide with an essential indication for assessing SGD dependent future changes to the coastal ecosystem with the environmental implications for the BoB as well as to the global ocean.

2. Study area

The study was conducted in the micro-tidal marshy coastal flat of Chandipur, Odisha, India adjoining the BoB (figure 1). Tidal height at the selected tidal coast varies with the lunar tidal cycle, submerging during high tide and emerging during low tide, with an extended >4 km intertidal zone (Mukherjee *et al.* 1987; Debnath *et al.* 2015). The tidal mudflat was morphologically characterized by recent paleo-aeolian dunes and recent alluvium deposits with overlying unconsolidated quaternary marine sediments and fluvio-deltaic deposits. The eastern part of the study area is covered by the River Budhabalanga (locally known as Buribalam), which is 4 km from the study site possibly have low discharge to the BoB in pre-monsoon and high in post-monsoon season due to seasonal rainfall variation.

2.1 *Hydroclimatology*

The average annual temperature of study location is 27°C with an annual variation of 13°–37°C. Annually the total rainfall is 1500 mm, and 70% of it occurs during the monsoonal months between late of June to end of September. Based on rainfall pattern, end of February to June is considered as pre-monsoon with average rainfall of 68 mm, July to September as monsoon accounts highest average rainfall of 215 mm and October to beginning of February as post-monsoon season have average rainfall of 34 mm. The average groundwater level fluctuates within 2–4 m below the ground level (bgl) in shallow upper unconfined aquifer. The higher meteoric recharge in monsoon season possibly aggravate the higher SGD rate 0.003–0.25 m^3 m^{-2} h^{-1} (Debnath *et al.* 2016) in post-monsoon season and no discharge to 0.15 m^3 m^{-2} h^{-1} SGD rate was a resultant of low rainfall recharge in pre-monsoon season (Debnath *et al.* 2016).

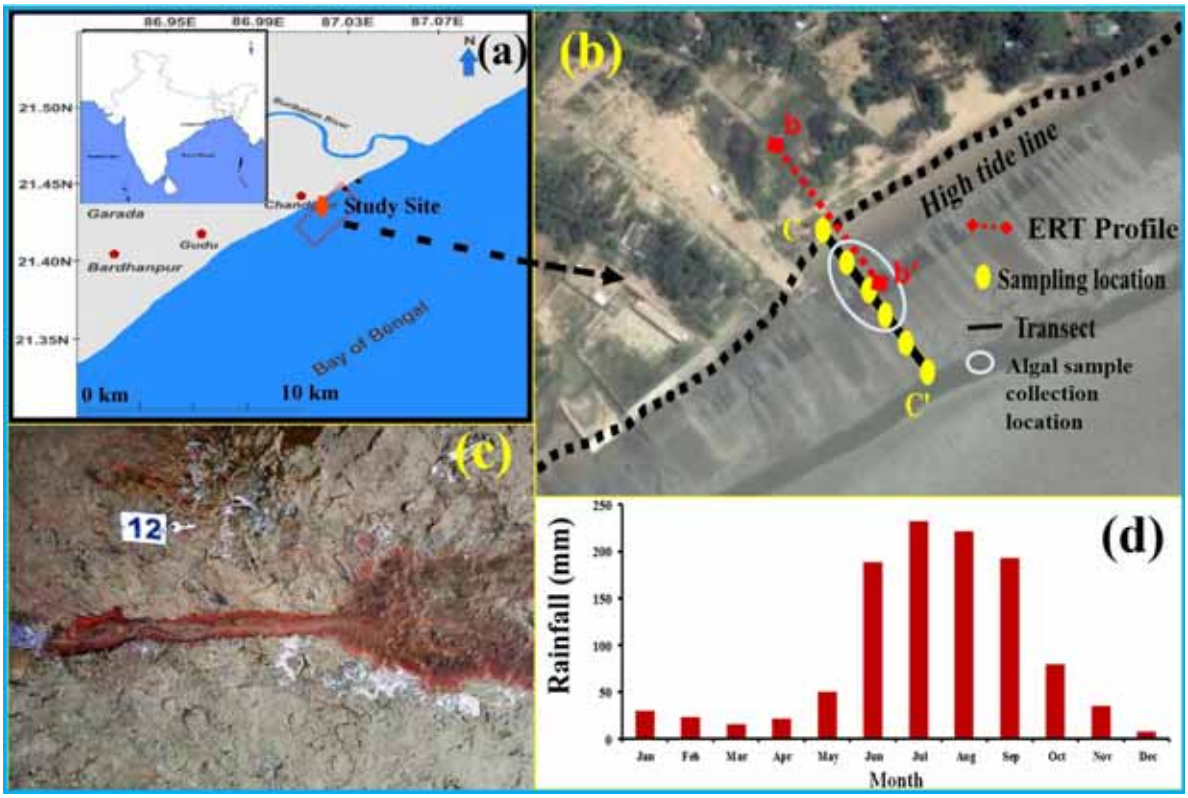

Figure 1. (**a**) Geographic location of the study site with location details (modified after Debnath *et al.* 2018). (**b**) Aerial view of the study sites with sampling locations of ERT profile (b–b′), SGD samples (both porewater and seepage water) (C–C′) and algal samples. (**c**) Representing the focused seepage point of respective study area with iron strain. (**d**) Monthly average rainfall distribution of last 36 yrs (1979–2015) of Chandipur, Orissa (modified after Debnath *et al.* 2018).

2.2 *Sampling and preservation*

Multi-depth (MD) porewater samples ($n = 42$) were collected up to 180 cm from surface with 30 cm below seabed level (bsbl) depth interval and spatial extension of 20 m distance interval from high tide line (HTL) to 100 m offshore distance. Seepage meter sampling was performed (n =120) by using seepage meter (Lee 1977). For seepage meter sampling 5 m distance interval was considered for HTL to 10 m offshore distance, 10 m distance interval was considered for 10–50 m offshore location, 15 m was considered for 50–90 m offshore location and considered farthest offshore location at 110 m (Debnath *et al.* 2015, 2019; Debnath and Mukherjee 2016). The details of the collected sample numbers and seasons are presented in table 1. Seepage meters were installed during the hydrologic year of 2014–2015, with a diurnal monitoring (over 9-hr) time periods for full lunar tidal and temporal scale (Debnath *et al.* 2015; Debnath and Mukherjee 2016). All the seepage meter samples were considered as SGD samples for the entire manuscript.

Water samples were collected in HDPE bottles both for the ionic and isotopic analysis. Isotopic samples were stored in 8 ml bottles without head space. For the analysis of ions, 60 ml samples were collected by following the standard hydrogeochemical protocols and standard preservatives (Wood 1981).

Algal samples were collected by grab sampling method. These (also known as point samples) are collected by inverting a container, placing it below the water surface, then turning it upright and allowing it to fill. Grab samples can also be taken quickly lowering a container 6 inches (15 cm) below the surface. Five algal samples were collected within 12 m of radius around the seepage face. This method can be used during a fish kill and when a lab-line is not available or practical. To preserve the algal samples 2 ml of Lugol's solution (mixture of Iodine and KI) was added and kept out of direct sunlight. Lugol's solution maintain the algal cell structure and prevent microbial decomposition (Fetscher *et al.* 2009).

2.3 *Hydrogeochemical analysis*

In *in-situ* condition salinity content was measured by using multi-parameter probe (HI929828, Hanna

Table 1. *Summary of collected samples both for MD porewater and seepage water.*

	Multi-depth (MD) porewater			Seepage meter		
Total sample	$n = 42$	Interval	Season	$n = 120$	Interval	Algae
Total depth	Surface to 180 cm	30 cm	Both for pre- and post-monsoon	Surface	–	A composite sample from 5 different locations from seepage face were collected within 12 m radius
Total offshore distance	HTL to 100 m*	20 m		HTL to 100 m	5 m interval → HTL to 10 m offshore 10 m interval → 10–50 m offshore 15 m interval → 50–90 m offshore and 110 m	

*Sample was collected from the 6 locations from the HTL to 100 m offshore distance.

Inc., USA). All the samples were filtered with 0.22 µm nylon filter paper, followed by the analysis of major anions (viz., Cl^-, SO_4^{2-} and NO_3^-) by ion chromatography (Metrohm-m IC 883 Plus, Metrohm-m, Switzerland). High salinity samples were analysed in high-end ion-chromatograph (Dionex 5000 series). Based on the salinity and TDS content, all the samples were diluted up to 20 times to enhance the analytical precision. Mg^{2+} concentration of the collected seepage samples was also analysed in ion chromatograph. Stable water isotopic analysis was done in high precision laser cavity ring-down spectrometry method (Piccaro Inc., model no: L2130-i) in high precision mode (Thorsen *et al.* 2011; Walker *et al.* 2016) at School of Environmental Science and Engineering, IIT Kharagpur. The precision of the measurements is less than ±0.1‰ for $\delta^{18}O$ (Debnath *et al.* 2019).

2.4 *Geophysical technique: Electrical resistivity tomography (ERT)*

Multi-electrode systems are commonly used for the acquisition of the electrical resistivity data sets. ERT was used in this SW–GW interaction study to examine the vertical-to-perpendicular to shoreline resistivity distribution on this aquifer media saturated with mixed water, which vary seasonally, in a proportion of fresh terrestrial water and seawater.

These automatically measure the apparent resistivity for a series of electrode combinations for a given array geometry. An ERT survey was conducted using 42 equally spaced electrodes with 5 m inter-electrode spacing, arranged in a Schlumberger array, along a survey line of 200 m perpendicular to the shoreline for both the seasons to determine the horizontal and vertical resistivity distribution (or its reciprocal – conductivity) of the aquifer. The midpoint of ERT profile is placed at HTL, therefore the profiles are having stretch of 100 m inland and 100 m offshore distance from HTL in both the seasons (figure 1). The stretch of the ERT profiles from the HTL to 100 m offshore distance was only considered and discussed in this study to compare with the geochemical data.

Each section of resistivity profiles was processed by the inversion of apparent resistivity (ra) by using the RES2DINV (Geotomo) 2Dfinite-element software, based on least-square inversion by a quasi-Newton method (Loke and Barker 1996). Total number of iteration done for the pre-monsoon profile was 54 with RMSE 11% and 53 for the post-monsoon profile with RMSE 8%.

2.5 *Culture conditions and growth of algae*

The L1 medium was prepared using natural Bay of Bengal (BoB) seawater. The medium was filtered with 0.22 µm Whatman® filter paper prior to use. The algal cultures were acclimatized at room temperature 25°C and at a constant light cycle (12 hr each light and dark) during exponential growth for 10 days. Growth was quantified as cell counts. 250 µl cultures were collected and cells were counted using Muse® Cell Analyzer Millipore® flow cytometer (López-Rosales *et al.* 2015). Glass wares and equipment used in this study were washed with 30% v/v Hydrochloric acid (HCl) followed by thorough rinse with autoclaved ultrapure (Type I)

Millipore® water to remove the metal and ammonium.

2.5.1 *Nutrient dependent growth dynamics of algae*

Batch culture experiments were conducted with an initial algal concentration of 300 cells/mL. The polystyrene multiwall plates were kept in incubator and illuminated by 60 W cool daylight fluorescent lights for 72 hrs at 25°C. The optimization of these experiment was conducted in triplicates. The medium was amended with different nitrate and glutamic acid varying from 0.5 to 100 µmol N/L (e.g., 0.5, 1, 5, 10, 50 and 100 µmol N/L). Growth rates μ (day-1) was calculated by following Guillard *et al.* (1973) using the following equation.

$$\mu = \{\ln(N_1) - \ln(N_0)\}/(T_1 - T_0), \quad (1)$$

where, N_1 and N_0 are the cell counts at T_1 and T_0, respectively, during exponential growth phase. The relationship between the specific growth rate and cell counts were fitted to Monod growth kinetics using the following equation:

$$\mu = \mu_{m.} S/(K_\mu + S), \quad (2)$$

where, μ is the specific growth rate (day-1), μ_m is the maximum specific growth rate (day-1), and S is the cell counts (µmol N/L). K_μ is the half saturation constant (µmol N/L) which is half of maximum specific growth rate. Nitrate and one essential amino acid glutamic acid (glu) were considered as sole source of nitrogen. According to Felbeck (1971) about 40–50% of nitrogen in the humic compounds is in amino acid form.

3. Results

3.1 *Variations of resistivity (ERT) along the study transect*

In the post-monsoon season, resistivity was recorded high at the top surface (8.0 Ωm up to 1 m depth), and then it decreased to 1.2 Ωm up to the depth of 26 m. At top of the surface, high resistivity delineate the saturated layer with terrestrial fresh groundwater fraction. Saturation of layer and resistivity range ∼8 Ωm was, might be due to discharge of high T-SGD in post-monsoon season and was a resultant of monsoonal meteoric recharge (Debnath *et al.* 2019). In the post-monsoon, the ERT values gradually decreased with the increasing depths (up to <2 Ωm). The resistivity was around 1.0 Ωm at the top of the surface along the transect in pre-monsoon season and highest was observed at 5.2 m depth which gradually decreased up to 27.8 m depth. Low resistivity in pre-monsoon season was a resultant of less terrestrial freshwater contribution to the discharging water and high recirculated marine water component (figure 2).

Spatially, ERT profiles showed that the resistivity got gradual decreases over the increasing offshore distance (figure 2). The variation of resistivity values in surficial sediments, and geometry of the mixed brackish and freshwater wedges varied seasonally due to potential loads of terrestrial freshwater component in discharging groundwater. Varied geomorphic patterns in aquifer and saturation with varied source water with depth possibly play a significant role in circulation pattern of terrestrially sourced groundwater and recirculated seawater even in seasonal scale (De Franco *et al.* 2009; Zarroca *et al.* 2014; Goebel *et al.* 2017).

3.2 *Geochemical evolutions along discharging flow path*

The maximum observed Cl^- content in seepage water sample was found to be 379 and 384 mM/L in pre- and post-monsoon season with a minimum of 24 and 21 mM/L. Low average Cl^- content was observed in post-monsoon than pre-monsoon season across the transect from HTL to 110 m offshore distance. Lower Cl^- content in post-monsoon than the pre-monsoon was a result of high terrestrial freshwater contribution to the discharging water due to monsoonal meteoric recharge, which limits the possible recirculation of infiltrated brackish water through the seepage faces during high tide time (Debnath *et al.* 2019). Average Mg^{2+} content was higher in post-monsoon (22.84 mM/L) than the pre-monsoon (19.99 mM/L) season was a resultant of higher terrestrial freshwater contribution to the discharging water. The terrestrial fresh groundwater was a main source of major solutes in SGD samples. Range of Mg^{2+} content varies between 3.3 and 39.8, and 2.9 to 40.4 mM/L in pre- and post-monsoon season, respectively (Debnath *et al.* 2018). The recorded Cl^- and Mg^{2+} was observed to be low at the nearshore location (within HTL to 30 m offshore distance), and gradually increases with increasing offshore distances with highest values at 110 m offshore distance. SGD samples have lowest Cl^- (<100

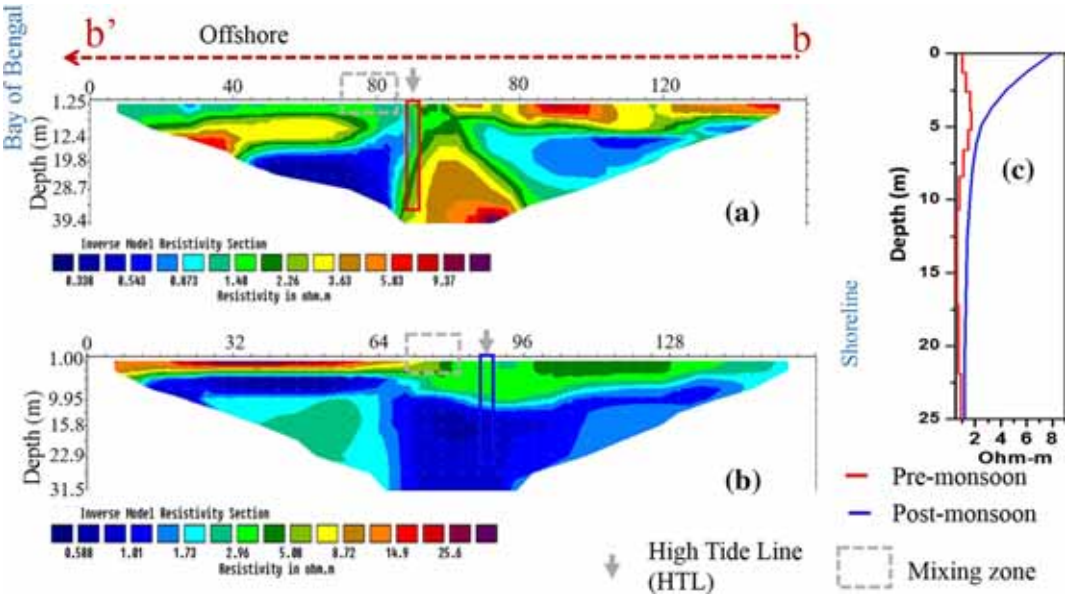

Figure 2. ERT profile perpendicular to the shoreline of Chandipur, Orissa of (**a**) pre-monsoon and (**b**) post-monsoon season, (**c**) representing the depth wise variations of resistivity in both the seasons. The middle point of the profile was located at the HTL. Presented data in sub-figure (c) are from the same spatial locations of both the profiles.

mg/L) content within 20 m offshore from HTL, in both seasons, respectively (Debnath *et al.* 2018).

The observed pre- and post-monsoonal range of NO_3^- content in SGD samples was 37–352 and 53–297 μM/L, respectively. Highest NO_3^- (an essential nutrient) concentration was observed in pre-monsoon season (352 μM/L) than the post-monsoon season (297 μM/L), but the average NO_3^- content was highest in pre-monsoon (157 μM/L) season than post-monsoon (141 μM/L) season. NO_3^- content of SGD samples in pre-monsoon season started decreasing below 100 μM/L from 50 m offshore to lowest (37.2 μM/L) at 110 m offshore distance. Post-monsoon season recorded >100 μM/L NO_3^- content of SGD samples up to 70 m offshore distance and then started decreasing up to 53.3 μM/L at 110 m offshore distance. Study results revealed that the higher NO_3^- is persisting with the low salinity zone where T-SGD fraction was high, which was possibly a reduced zone, where it undergoes denitrification process and limits the NO_3^- content with the SGD through the far offshore distances, where SGD mixes with the recirculated brackish water and may also depend on advective transport and freshwater discharge rate (Slomp and Van Cappellen 2004; Kroeger and Charette 2008). The SO_4^{2-} content varied within the range of 2.3–17.9 and 2.2–18.1 mM/L in pre- and post-monsoon seasons, respectively, with higher average in post-monsoon (avg. 10.66 mM/L) than pre-monsoon (avg. 9.44 mM/L) season. The range of Br^- content was 4.1–49.3 and 4.1–48.9 mM/L in pre- (avg. 23.21 mM/L) and post-monsoon (avg. 28.47 mM/L) season, respectively. The SO_4^{2-} and Mg^{2+} content was recorded lowest at nearshore locations, and rising up to its highest concentration in SGD samples at far offshore location at 110 m (figure 3).

The $\delta^{18}O$ content of the SGD samples ranged from −3.63 to +2.586‰ and −5.03 to −2.27‰ in pre- and post-monsoon season. Highest depleted $\delta^{18}O$ values was observed at an offshore distance of 15 m in pre-monsoon season, whereas at 45 m offshore distance in post-monsoon season. Meteoric water recharge and presence of fresh groundwater component in discharging groundwater may deplete the $\delta^{18}O$ composition of SGD samples in post-monsoon in comparison to pre-monsoon season, respectively (Debnath *et al.* 2019). Possibly local meteoric recharge and regional groundwater play a crucial role in essential nutrient and solute transport to the marine ecosystems.

3.3 *Geochemical processes of discharging porewater along depth*

At the top of the seepage face MD porewater samples have a minimum NO_3^- content at 40 m offshore distance in pre-monsoon season, while in post-monsoon season lowest was observed at >60 m offshore and have low concentration up to 110 m offshore distance in both of the seasons,

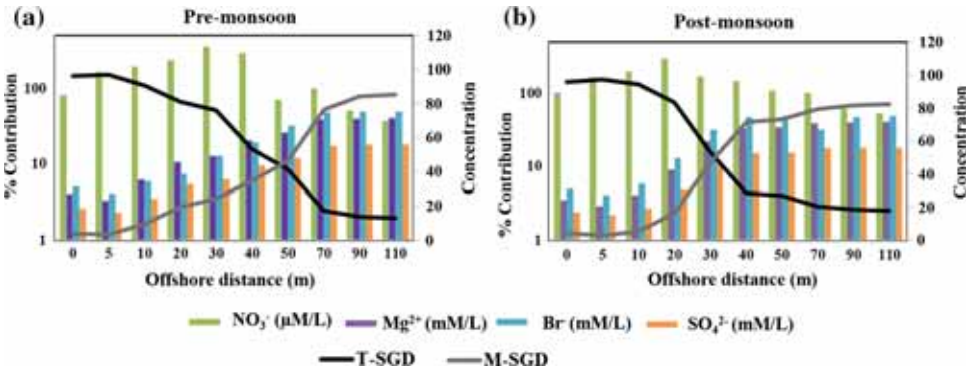

Figure 3. Variations of solutes and nutrients along offshore distance from HTL to 110 m offshore distance with T-SGD and M-SGD component in both (**a**) pre-monsoon and (**b**) post-monsoon season (modified after Debnath *et al.* 2015, 2018).

respectively. The highest NO_3^- content was observed at a depth of 30 cm bsbl at 40 m offshore distance in both pre-monsoon (119 µM/L) and post-monsoon season (148 µM/L). Average NO_3^- concentration in MD porewater samples varies with overall depths and offshore distances. Average NO_3^- concentration of MD porewater samples was observed highest around nearshore location and shallow depths, it gradually decreases with increasing offshore distances and depths in both of the seasons respectively (figure 4).

Cl^- content of major solutes also varies with the depth and distances. Average Cl^- concentration started increasing (>100 mM/L) from the 30 m offshore distances in pre-monsoon seasons, while from the 40 m offshore distances in post-monsoon season. With the increasing depths, the Cl^- concentration was also gradually decreasing. Highest Cl^- concentration was recorded at 100 m offshore distance at a depth of 180 cm bsbl in pre-monsoon season, while in post-monsoon season maximum (Cl^-: 455 mM/L) occurred at a depth of 30 cm bsbl and at 100 m offshore distance (figure 4). Minimum Cl^- concentration was observed at 180 cm bsbl at HTL in both pre- (16 mM/L) and post-monsoon (Cl^-: 6 mM/L) seasons.

3.4 *Growth kinetics of algal population*

Nutrient enrichment especially nitrogen source has been detected as a most influential factor for the growth of algal population primarily dinoflagellates. However, different dinoflagellates have specific affinity towards nitrogen source. It has been observed that the consortium of dinoflagellates was more inclined towards nitrate source than that of other studied sources. As the nitrate concentration increases in L1 medium, the cell counts increased by 71.46% approximately. In this batch culture experiments, dinoflagellates consortium grew well on nitrate rich media when they were supplied as the sole source of nitrogen. Maximum growth rate calculated from Monod kinetic model has been accumulated in table 2 for four samples in different nitrate and glutamic acid concentration. Eutrophic environment with higher nutrient concentration is responsible for dinoflagellates population and the formation of algal blooms across the study area.

4. Discussions

4.1 *Seasonal porewater displacement patterns*

The variations of freshwater zone up to higher depth in a meter scale was delineated by the resistivity data, while in shallow depth Cl^- content defined the sub-meter scale variations in a fine resolution in combination with ERT (figure 2). In a sub-meter scale, SGD with higher terrestrial freshwater fraction have higher resistivity, whereas the area saturated with saline water have low resistivity background. This variation of resistivity in the aquifer across the distance and depth depends on the discharging terrestrial freshwater load and hydraulic properties of the medium (Zarroca *et al.* 2014). In the present study, resistivity data with lithological variations showed a brackish water saturated sandy clay and fine sand zone as top layer within the depth of 1.5 mbgl. Overlaying of high resistivity zone by the low resistivity zone identified as a seawater encroaching zone, which varies seasonally. The overlying high resistivity zone was interpreted as freshwater discharge zone, which was highest in post-monsoon than pre-monsoon season. Excluding the influence

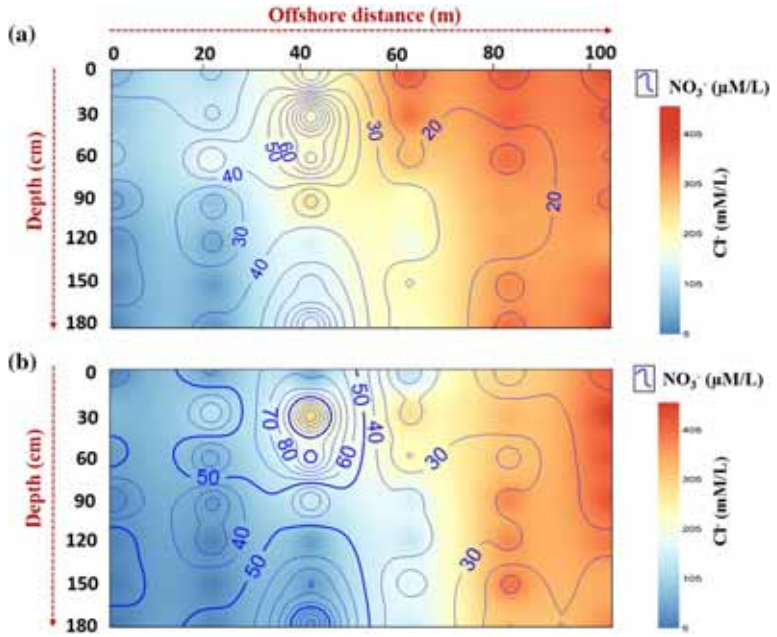

Figure 4. NO_3^- and Cl^- concentration variation along offshore distance and depth of porewater samples in (**a**) pre-monsoon season and (**b**) post-monsoon season (modified after Debnath *et al.* 2019).

Table 2. *The maximum specific growth rate and half saturation constant and affinity for each nitrogen compound was calculated following Monod kinetics model.*

Nitrogen sources as NO_3^- and glutamic acid	Sample	μ_m	K_μ	Affinity (μ_m/K_μ)	R^2
Nitrate	S1	1.78 ± 0.03	0.89 ± 0.02	1.93 ± 0.03	0.37
	S2	2.36 ± 0.04	1.18 ± 0.02	2 ± 0.05	0.69
	S3	2.3 ± 0.02	1.14 ± 0.03	2.02 ± 0.03	0.7
	S4	2.1 ± 0.01	1.1 ± 0.01	1.9 ± 0.01	0.71
	S5	2.3 ± 0.02	1.13 ± 0.03	2.02 ± 0.02	0.7
Glutamic acid	S1	1.89 ± 0.04	0.95 ± 0.02	1.98 ± 0.03	0.76
	S2	1.9 ± 0.02	0.96 ± 0.02	1.97 ± 0.05	0.75
	S3	1.94 ± 0.02	0.93 ± 0.03	2.08 ± 0.01	0.38
	S4	1.93 ± 0.01	0.97 ± 0.02	1.98 ± 0.02	0.74
	S5	1.94 ± 0.02	0.93 ± 0.03	2.08 ± 0.01	0.38

of depth, along the discharge path where groundwater converges with the seawater shows change in resistivity from high to low. Although sediment texture has strong influence on resistivity, the influence of saturated water in terms of saline or fresh suppress the influence of sediment structure (Zarroca *et al.* 2011, 2014). The changes in geomorphic patterns in aquifer system and saturation with fresh groundwater and brackish water with depth and seasons showed a significant circulation pattern through the seepage face. Although sediment texture strongly influences resistivity, the influence of water (both fresh and saline) saturated the pore spaces have higher influence than sediment structure (Zarroca *et al.* 2011, 2014).

The changes in resistivity across the distance and depths delineates the zone of mixing, where fresh SGD mixes with the recirculated seawater (figure 2). The variations in resistivity caused by the upwelling and discharge of freshwater from nearshore to far offshore distance. The change of resistivity in zone of convergence of fresh SGD with seawater was more evident in both the seasons (figure 2). Specifically, the changes in higher resistivity (ERT) values were extending up to 45 m

offshore distances in post-monsoon, whereas, in pre-monsoon season it extends only up to ∼30 m offshore distances, for the shallow sub-meter scale variations was the only possible zone of convergence. Excluding the influence of depth, along the discharge path where groundwater converges with the seawater shows change in resistivity from high to low (figure 2).

4.2 *Spatial and temporal variations of solute concentration of SGD*

Variability of concentrations of Cl^-, and $\delta^{18}O$ of SGD samples were used to find out the freshwater contribution in major solutes and nutrient discharge to the ocean. Possible freshwater discharge from the HTL to 20 m offshore have lower Cl^- content (<100 mg/L), started increasing from the 30 m offshore possibly where freshwater mixes with the seawater by infiltration through seepage faces. Low Cl^- content up to 20 m offshore distance is a result of high T-SGD input, which have low salinity. This higher terrestrial freshwater flux inhibits the infiltration of the recirculated marine component at the nearshore zone, whereas, with increasing offshore distances (>30 m) terrestrial input get lower and infiltration of higher marine component takes place and eventually increase the Cl^- content (Debnath *et al.* 2019). Cl^- content get saturated (>300 mg/L) in both the seasons from >70 to 110 m offshore distance. The changes $\delta^{18}O$ composition of discharged samples have distinct depleted signature in nearshore locations (HTL to 40 m) while get enriched with the increasing offshore distances (from 40 to 110 m) in pre-monsoon season (Debnath *et al.* 2019). The $\delta^{18}O$ composition of SGD samples were distinctly depleted in post-monsoon season than the pre-monsoon season (figure 5a and b). The highly depleted $\delta^{18}O$ values (> –3 ‰) suggests the freshwater sourced SGD was dominant in post-monsoon than the pre-monsoon season (Debnath *et al.* 2019). Results revealed that T-SGD > Marine derived SGD (M-SGD) always have depleted $\delta^{18}O$ composition in nearshore location and in further offshore distances M-SGD > T-SGD have enriched $\delta^{18}O$ composition (figure 5a–d).

Observed highest NO_3^- content at nearshore location have depleted $\delta^{18}O$ signature and got lower NO_3^- content with enriched $\delta^{18}O$ signature at far offshore distance (40–110 m) in both the seasons (figure 5e and f), although the quantity of nutrient depends on terrestrial and marine component, which varies with the discharge rate even in seasonal scale. The highest NO_3^- content (353 μM/L) was observed at 30 m offshore distance, when $\delta^{18}O$ signature was –1.85‰ and lowest NO_3^- (37 μM/L) at 110 m offshore with enriched $\delta^{18}O$ signature (+0.26‰) in pre-monsoon season. Highest NO_3^- content (298 μM/L) was observed at 20 m offshore distance with depleted $\delta^{18}O$ composition (–4.65‰) and lowest (NO_3^-: 53 μM/L) at far offshore (110 m) with relatively enriched $\delta^{18}O$ composition (–3.48‰) in post-monsoon season. Concentration of major solutes and nutrients of SGD was possibly dependent on the oxidation state of groundwater and the biogeochemical reaction undergoes through the source to discharge face. The higher content of NO_3^- was always aggravated with the suboxic to anoxic zone, where SGD rate was high and it undergoes through denitrification process (Slomp and Van Cappellen 2004; Kroeger and Charette 2008). Due to the denitrification processes the content NO_3^- was gradually decreased with increasing offshore distances. The release of other redox sensitive nutrients like SO_4^{2-} is also dependent on the redox reactions and mineralization process which may inhibit the transport of nutrients, is variable all through the shore-perpendicular directions (Charette *et al.* 2005; Jung *et al.* 2009; McAllister *et al.* 2015). Excluding the redox reactions and presence of reactive barrier, Br^-, SO_4^{2-} and Mg^{2+} content with low M-SGD at nearshore locations and higher content with high M-SGD at far offshore location suggests, that the recirculated marine water which mixed with the SGD along the mixing zone was the main source of it (figure 3). The higher regional groundwater contribution in post-monsoon seasons reflects from depleted $\delta^{18}O$ signature with lower Cl^- content and higher NO_3^- content in SGD samples than the samples from the pre-monsoon season (figure 5e–h).

4.3 *Variability of NO_3^- and Cl^- content in porewater samples*

The depth-wise variability of NO_3^- with Cl^- content is presented in figure 4. The low Cl^- content was observed within nearshore at top surface, whereas, with increasing depth and the spatial extension shows increasing Cl^- content. In pre-monsoon season low Cl^- content (∼100 mM/L) extends up to 20 m at top surface and >40 m at 180 cm depth, while in post-monsoon season it extends

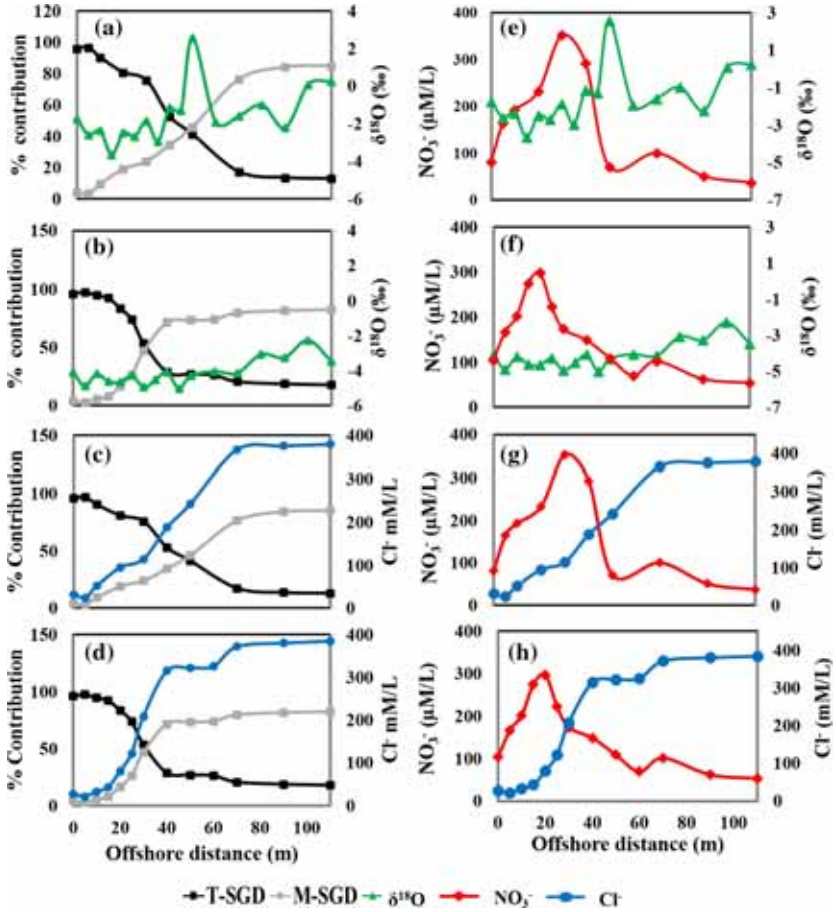

Figure 5. Variations of $\delta^{18}O$ signature along offshore distance from HTL to 110 m offshore distance with T-SGD and M-SGD component in both (**a**) pre-monsoon and (**b**) post-monsoon season. Variations of Cl^- concentration along offshore distance from HTL to 110 m offshore distance with T-SGD and M-SGD component in both (**c**) pre-monsoon and (**d**) post-monsoon season. Variations of NO_3^- concentration along offshore distance from HTL to 110 m offshore distance with $\delta^{18}O$ signature in both (**e**) pre-monsoon and (**f**) post-monsoon season. Variations of NO_3^- concentration along offshore distance from HTL to 110 m offshore distance with Cl^- concentration in both (**g**) pre-monsoon and (**h**) post-monsoon season (modified after Debnath *et al.* 2018, 2019).

up to 40 m at top surface and 50 m at bottom (180 cm) (figure 4). The occurrence of NO_3^- in multi-depth (MD) porewater samples was high with low Cl^- content. Spatially the NO_3^- content was observed high at nearshore locations and gradually decreases with increasing offshore distance. More interestingly the NO_3^- content was observed high at the top of the seepage faces, and gradually decreases with increasing depths for both seasons.

4.4 *Occurrence of algal population in BoB*

The most abundant and frequently detected group of organisms in the marine environment is dinoflagellates. The metabolism of this group of algae has rarely been explored in comparison to other micro-algae such as cyanobacteria and diatoms (Guillard and Keller 1984). In comparison with the present study nitrogen limiting phytoplankton was also reported in studies of eastern and western coast of India (Achary *et al.* 2014; Baliarsingh *et al.* 2015), although, the dynamics and the growth of the nutrient dependent species was not reported. This present study is one of the first to document the occurrence of micro-algae at the SW–GW mixing zone where SGD was one of the major sources of nutrient (NO_3^-) supply and their growth dynamics in laboratory condition. All of the samples showed similar patterns of algal and microalgal population, as most of them are the nitrogenous source dependent, which brings out the preliminary knowledge on algae population across the coastal area of BoB. Stable variation, abundance and species diversity of dinoflagellates community

were observed in all samples collected in close proximity. Altogether, 31 species of dinoflagellates were detected, among them, *Oxytoxum* sp. and *Gonyaulax grindleyi* were the most abundant species, followed by *Gonyaulax monospina* (figure 6a). During the period of the study, approximately 10 species of deleterious microalgae were identified. The percentage of various groups of dinoflagellates constituting the blooms during post-monsoon season is presented in figure 6. Approximately 5.2% of the samples contain *Gonyaulax scrippsae* followed by *Amphisolenia bidentata* and *Amphisolenia globifera* which occupy more than 3% of the dinoflagellate's population. *Alexandrium* sp., *Amphidinium* sp., *Gambierdiscus* sp. and *Gonyaulax polyedra*, *Gonyaulax polygramma* were detected in a negligible quantity. More than 30% of the dinoflagellates belong to *Oxytoxum* sp.

4.5 *Contribution of SGD derived nutrient loads to BoB: Implication to the global ocean*

SGD is an important source of nutrients to the coastal areas of BoB and the diversity/abundance of coastal ecology mostly depends on it. A previous study by Debnath *et al.* (2018) also explained the occurrence of low concentration total iron (Fe_{tot}) at nearshore location and with relatively low pH was a T-SGD sourced discharge. Reduced iron (Fe^{2+}) with low salinity in SGD samples was an indication of terrestrial derived nutrient discharge to the marine system (Debnath *et al.* 2018). Along with the NO_3^- the estimated annual SGD sourced Fe_{tot} flux to the BoB was 224 mM m^{-2} day^{-1} (Debnath *et al.* 2018). In context of the global studies, the NO_3^- flux is significantly comparable with the studies conducted in Sunset State Beach, California, (fluxes were found to be 2.6–3.9 M m^{-1} day^{-1}, Lecher *et al.* 2015), San Francisco Bay ($\leq$0.7 M m^{-1} day^{-1}, Lecher *et al.* 2015), and Stinson Beach of California (1.4−2.4 M m^{-1} day^{-1}, Nicholas *et al.* 2008). In the present study, the supply of NO_3^- to BoB is lower in comparison with the global studies, and it is one of the responsible factors for less productivity of BoB (Prasanna *et al.* 2002, 2004; Singh and Chaturvedi 2010). The presence of the benthic algae and their nitrogenous nutrient supply is mostly dependent on the SGD fluxes (Boyton and Kemp 1985; Kimberly *et al.* 2012; Lecher *et al.* 2015).

4.6 *Implication of SGD derived nutrient dynamics to coastal ecology*

SGD derived nutrients along with atmospheric, terrigenous, and oceanic sourced nutrients have a

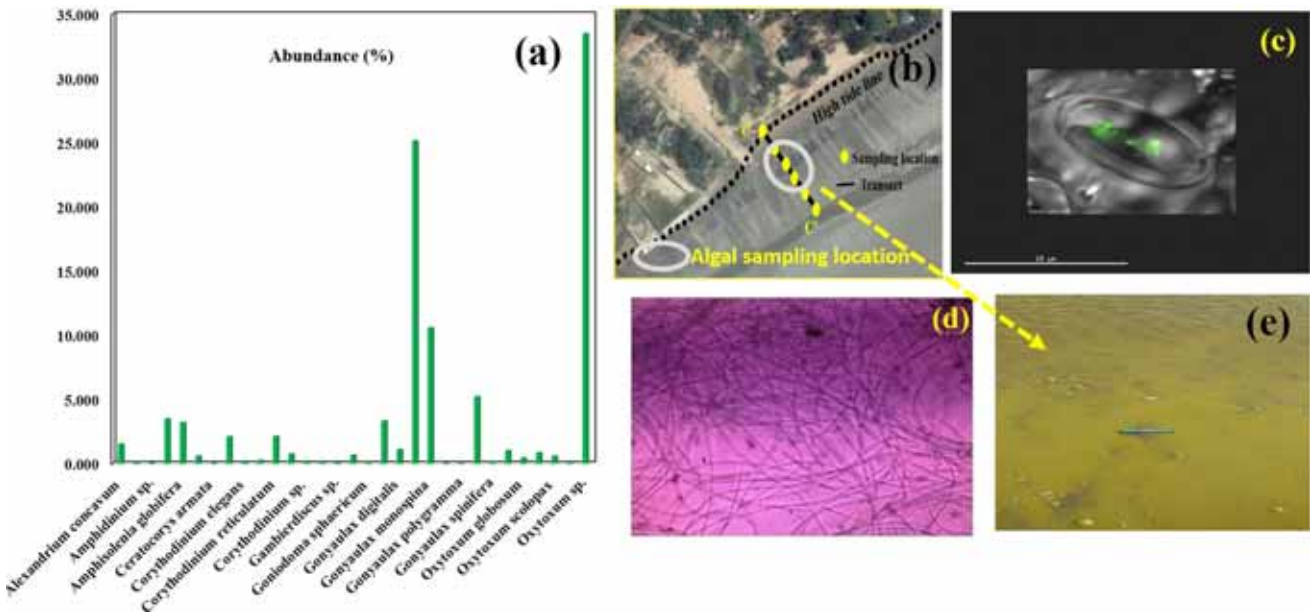

Figure 6. (**a**) Abundance of identified algal species along the discharge zone from a composite sample. (**b**) The figure shows the location of algal sample collection within the study area and period. (**c**) Image of *Cladophora* sp. and (**d**) image of *Phormidium* sp.: These are auto-fluorescence images of algae viewed in life cell cytometry (**b**, **c** and **d** were modified after Debnath and Mukherjee 2016), (**e**) representing the dense algal mats over the seepage face.

control on the primary productivity of the marine ecosystems (Pearl 1997; Sugimoto *et al.* 2015). SGD contribute huge amount of required nutrients to the global ocean. Availability of essential nutrients corresponds to the composition of diatoms, were primary producers in a marine ecosystem (Sugimoto *et al.* 2015).

The BoB receives freshwater influx in the amount of average $\sim 1.5\times10^{12}$ m^3 from major rivers (Irrawady, Brahmaputra, Ganges and Godavari) (UNESCO 1988; Gomes *et al.* 2000), while, SGD counters only 6–10% of the global surface water input. The freshwater flux from the river to the BoB was considered as the major controlling factor for the transportation of major solutes/nutrient, and have major control over the productivity of ocean, although, the BoB was considered as less biologically productive due to limited supply of nutrients (Prasanna *et al.* 2002, 2004; Singh and Chaturvedi 2010). In comparison with the riverine input only 6–10% of SGD flux have a considerable influence on nutrient supply and ecological enrichment, and the estimated flux of NO_3^- is 8.76×10^8 mM m^{-2} yr. This study suggests that process based supply of SGD derived nutrients is an essential factor controlling algal growths and eutrophication events, even in regional ecosystem dynamics in coastal areas (figure 6a and b) (Null *et al.* 2012). Supply of NO_3^- content and DIN_{tot} (total dissolve inorganic nitrogen)(not studied in present work) have plausible influence on primary biological productivity. Discharged nutrient have a significant role on primary productivity, which is directly associated with phytoplankton dynamics and size. The identified phytoplankton colonies are dominated by the *Phormidium* sp., *Navicula* sp., *Mastogloia* sp., *and Chameosiphn* sp. (figure 6c and d) in the studied area (Debnath and Mukherjee 2016). The mentioned diatom groups are 'plankton functional types' have control on biogeochemical cycles of the marine ecosystem (Totterdell *et al.* 1993). These diatom groups have wide number of diverse species (Mann 1999), and counted for the overall marine primary productivity (Tréguer *et al.* 1995; Smetacek 1999). However, we did not evaluate influence of P-dependent growth of these groups and/or species of phytoplankton, which may vary spatially from the nearshore to far offshore distance and temporally in our studied area to understand influence of SGD in marine biogeochemical productivity.

5. Conclusion

The SGD to the BoB is dominated by the T-SGD in post-monsoon, and M-SGD in pre-monsoon season. T-SGD is restricted to nearshore location in pre-monsoon, while it extends up to the offshore location from HTL in post-monsoon. The discharge in both of the seasons is controlled by the terrestrial freshwater load. The present work illustrates that the SGD associated nutrient supply to the BoB, varies temporally and spatially at this tidal mudflat. The discharge of essential nutrients and solutes gives rise to very rich and diverse biota and enhances the biological productivity of the marine ecosystem. The seasonal isotope and Cl^- data portrays different aspects of local water balance: (a) high rate of seawater infiltration through seepage face during pre-monsoon, (b) a net-terrestrial input from regional groundwater during post-monsoon and (c) discharge of more nutrient rich freshwater component during monsoon season, which mixes with seawater in far offshore distance and again discharges into the ocean without affecting the nutrient content. The salinity of seepage-meter and porewater samples illustrates that the SGD at this site is non-uniform in terms of solute composition and the volume of discharged groundwater. The ecohydrological response to this solute flux results in occurrence of N-sensitive dinoflagellates and some haptophytes, with greenish and brownish hue that provides a distinct look to the coastal landscape. This study results would depict the occurrence of nutrients in SW–GW mixing zones and its possible implications to the nutrient derives algal blooms adjoining to the tropical ocean.

Acknowledgements

Authors are thankful to Thermo Fisher Scientific team for their sincere help in preparation of such high salinity samples and analysis. Financial support for this work was provided by Indian Institute of Technology (IIT)-Kharagpur and Ministry of Earth Science, Government of India (vide nos. MOES/PAMC/H&C/23/2013-PC-II and MOES/PAMC/H&C/103/2017-PC-II).

References

Achary M S, Panigrahi S, Satpathy K K, Sahu G, Mohanty A K, Selvanayagam M and Panigrahy R C 2014 Nutrient

dynamics and seasonal variation of phytoplankton assemblages in the coastal waters of southwest Bay of Bengal; *Environ. Monit. Assess.* **186(9)** 5681–5695.

Baliarsingh S K, Srichandan S, Naik S, Sahu K C, Lotliker A A and Kumar T S 2015 Seasonal variation of phytoplankton community composition in coastal waters off Rushikulya Estuary, east coast of India.

Beck A J, Alex A K, Jena L L and Michele C A 2015 Chemical flux associated with spatially and temporally variable submarine groundwater discharge, and chemical modification in the Subterranean Estuary at Gloucester Point, VA (USA), *Estuar. Coast.*, https://doi.org/10.1007/s12237-015-9972-0.

Boyton W R and Kemp W M 1985 Nutrient regeneration and oxygen consumption by sediments along an estuarine salinity gradient; *Mar. Ecol. Prog. Ser.* **23** 45–55.

Charette M A, Sholkovitz E R and Hansel C M 2005 Trace element cycling in a subterranean estuary: Part 1. Geochemistry of the permeable sediments; *Geochim. Cosmochim. Acta* **69** 2095–2109.

Das K and Mukherjee A 2019 Depth-dependent groundwater response to coastal hydrodynamics in the tropical, Ganges river mega-delta front (the Sundarbans): Impact of hydraulic connectivity on drinking water vulnerability; *J. Hydrol.* **575** 499–512.

De Franco R, Biella G, Tosi L, Teatini P, Lozej A, Chiozzotto B and Giada M *et al.* 2009 Monitoring the saltwater intrusion by time lapse electrical resistivity tomography: The Chioggia test site (Venice Lagoon, Italy); *J. Appl. Geophys.* **69(3–4)** 117–130.

Debnath P and Mukherjee A 2016 Quantification of tidally-influenced seasonal groundwater discharge to the Bay of Bengal by seepage meter study; *J. Hydrol.* **537** 106–116.

Debnath P, Das K, Mukherjee A, Ghosh N C, Rao S, Kumar S, Krishnan G and Joshi G 2019 Seasonal-to-diurnal scale isotopic signatures of tidally-influenced submarine groundwater discharge to the Bay of Bengal: Control of hydrological cycle on tropical oceans; *J. Hydrol.* **571** 697–710.

Debnath P, Mukherjee A and Das K 2018 Characterization of tidally-influenced seasonal nutrient flux to the Bay of Bengal and its implications on the coastal ecosystem; *Hydrol. Process.* **32(9)** 1282–1300.

Debnath P, Mukherjee A, Singh H K and Mondal S 2015 Delineating seasonal porewater displacement on a tidal flat in the Bay of Bengal by thermal signature: Implications for submarine groundwater discharge; *J. Hydrol.* **29(3)** 1185–1197.

Fetscher A E, Busse L and Ode P R 2009 Standard operating procedures for collecting stream algae samples and associated physical habitat and chemical data for ambient bioassessments in California, California State Water Resources Control Board Surface Water Ambient Monitoring Program (SWAMP) Bioassessment SOP, June 10, 2009, **2**.

Goebel M, Pidlisecky A and Knight R 2017 Resistivity imaging reveals complex pattern of saltwater intrusion along Monterey coast; *J. Hydrol.* **551** 746–755.

Gomes H R, Goes J I and Saino T 2000 Influence of physical processes and freshwater discharge on the seasonality of phytoplankton regime in the Bay of Bengal; *Cont. Shelf Res.* **20(3)** 313–330.

Gonneea M E, Morris P J, Dulaiova H and Charette M A 2008 New perspectives on radium behavior within a subterranean estuary; *Mar. Chem.* **109** 250–267.

Hwang D W, Kim G, Lee Y W and Yang H S 2005 Estimating submarine inputs of groundwater and nutrients to a coastal bay using radium isotopes; *Mar. Chem.* **96** 61–71.

Johannes R E 1980 The ecological significance of the submarine discharge of groundwater; *Mar. Ecol. Prog. Ser.* **3** 365–373.

Jung H B, Charette M A and Zheng Y 2009 Field, laboratory, and modeling study of reactive transport of groundwater arsenic in a coastal aquifer; *Environ. Sci. Technol.* **43** 5333–5338.

Kimberly N, Natasha A, Dimova T, Karen L, Knee, Esser B K, Swarzenski P W, Singleton M J, Stacey M and Paytan A 2012 Submarine groundwater discharge-derived nutrient loads to San Francisco Bay: Implications to future ecosystem changes; *Estuar. Coast.* **35(5)** 1299–1315.

Kroeger K D and Charette M A 2008 Nitrogen biogeochemistry of submarine groundwater discharge; *Limnol. Oceanogr.* **53(3)** 1025–1039.

Lecher A L, Mackey K, Kudela R, Ryan J, Fisher A, Murray J and Paytan A 2015 Nutrient loading through submarine groundwater discharge and phytoplankton growth in Monterey Bay, CA; *Environ. Sci. Technol.* **49(11)** 6665–6673.

Lee D R 1977 A device for measuring seepage flux in lakes and estuaries; *Limnol. Oceanogr.* **22(1)** 140–147.

Loke M H and Barker R D 1996 Rapid least-squares inversion of apparent resistivity pseudosections by a quasi-Newton method 1; *Geophys. Prospect.* **44(1)** 131–152.

López-Rosales L, García-Camacho F, Sánchez-Mirón A, Contreras-Gómez A and Molina-Grima E 2015 An optimisation approach for culturing shear-sensitive dinoflagellate-microalgae in bench-scale bubble column photobioreactors; *Bioresour. Technol.* **197** 375–382.

Mann D G 1999 The species concept in diatoms; *Phycologia* **38(6)** 437–495.

McAllister, Sean M, Barnett J, Heiss J W, Findlay A J, MacDonald D J, Dow C L, Luther G W III, Michael H A and Chan C S 2015 Dynamic hydrologic and biogeochemical processes drive microbially enhanced iron and sulfur cycling within the intertidal mixing zone of a beach aquifer; *Limnol. Oceanogr.* **60(1)** 329–345.

Michael H A, Mulligan A E and Harvey C F 2005 Seasonal oscillation in water exchange between aquifers and the coastal ocean; *Nature* **436** 1145–1148.

Miller D and Ullman W 2004 Ecological consequences of ground water discharge to Delaware Bay, United States; *Groundwater* **42** 959–970.

Mukherjee K K, Das S and Chakrabarti A 1987 Common physical sedimentary structures in a beach-related open sea siliciclastic tropical tidal flat at Chandipur, Orissa and evaluation of weather conditions through discriminate analysis; *Senckenbergiana Maritime* **19** 261–293.

Null K A, Dimova N T, Knee K L, Esser B K, Swarzenski P W, Singletoon M J, Stacey M and Paytan A 2012 Submarine groundwater discharge-derived nutrient loads to San Francisco bay: Implications to future ecosystem changes; *Estuar. Coast.*, https://doi.org/10.1007/s12237-012-9526-7.

Prasanna K S, Muraleedharan P M, Prasad Gauns, T G, Ramaiah M N, De Souza S N, Sardesai S and Madhupratap M 2002 Why is the Bay of Bengal less productive during summer monsoon compared to the Arabian Sea?; *Geophys. Res. Lett.* **29(24)** 881–884.

Prasanna K S, Nuncio M, Narvekar J, Kumar A, Sardesai D S, De Souza S N, Gauns M, Ramaiah N and Madhupratap M

2004 Are eddies nature's trigger to enhance biological productivity in the Bay of Bengal?: *Geophys. Res. Lett.* **31(7)**, https://doi.org/10.1029/2003GL019274.

Rapaglia J, Beck A, Stieglitz T, Bokuniewicz H and Kontar E 2006 Submarine groundwater discharge patterns through volcanic fractured rock. Submarine Groundwater Discharge Assessment Intercomparison Experiment, Mauritius, Report to UNESCO.

Rocha C, Wilson J, Scholten J and Schubert M 2015 Retention and fate of groundwater-borne nitrogen in a coastal bay (Kinvara Bay, Western Ireland) during summer; *Biogeochem.* **125** 275–299.

Roy M, Martin J B, Cherrier J, Cable J E and Smith C G 2010 Influence of sea level rise on iron diagenesis in an east Florida subterranean estuary; *Geochim. Cosmochim. Acta* **74(19)** 5560–5573.

Simmons G M 1992 Importance of submarine groundwater discharge and seawater cycling to material flux across sediment/water interfaces in marine environments; *Mar. Ecol. Prog. Ser.* **84** 173–184.

Singh R P and Chaturvedi P 2010 Comparison of chlorophyll concentration in the Bay of Bengal and the Arabian Sea using IRS-P4 OCM and MODIS Aqua.

Slomp C P and Van Cappellen P 2004 Nutrient inputs to the coastal ocean through submarine groundwater discharge: Controls and potential impact; *J. Hydrol.* **295** 64–86.

Smetacek V 1999 Diatoms and the ocean carbon cycle; *Protist* **150(1)** 25–32.

Sugimoto R, Honda H, Kobayashi S, Takao Y, Tahara D, Tominaga O and Taniguchi M 2015 Seasonal changes in submarine groundwater discharge and associated nutrient transport into a tideless semi-enclosed embayment (Obama Bay, Japan); *Estuar. Coast.* **39(1)** 13–26.

Tamborski J J, Cochran J K and Bokuniewicz H J 2017 Submarine groundwater discharge driven nitrogen fluxes to Long Island Sound, NY: Terrestrial *vs.* marine sources; *Geochim. Cosmochim. Acta* **218** 40–57.

Thorsen T, Shriver T, Racine N, Richman B A and Schoeller D A 2011 Doubly labeled water analysis using cavity ring-down spectroscopy; *Rapid Comm. Mass Spectrom.* **25(1)** 3–8.

Totterdell I J, Armstrong R A, Drange H, Parslow J S, Powell T M and Taylor A H 1993 Trophic resolution. Towards a Model of Ocean Biogeochemical Processes, NATO ASI **1** 10 p.

Tréguer P, Nelson D M, Van Bennekom A J, DeMaster D J, Leynaert A and Quéguiner B 1995 The silica balance in the world ocean: A reestimate; *Science* **268** 375–379.

Valiela I, Bowen J L and Kroeger K D 2002 Assessment of models for estimation of land derived nitrogen loads to shallow estuaries; *Appl. Geochem.* **17** 935–953.

Walker S A, Azetsu-Scott K, Normandeau C, Kelley D E, Friedrich R, Newton R and Craig S E 2016 Oxygen isotope measurements of seawater ($^{18}O/^{16}O$): A comparison of cavity ring-down spectroscopy (CRDS) and isotope ratio mass spectrometry (IRMS); *Limnol. Oceanogr.-Meth.* **14(1)** 31–38.

Wood W W 1981 Guidelines for collection and field analysis of groundwater samples for selected unstable constituents. Techniques of Water-Resources Investigations of the United States Geological Survey Book 1, Chapter D2, 11.

Zarroca M, Bach J, Linares R and Pellicer X M 2011 Electrical methods (VES and ERT) for identifying, mapping and monitoring different saline domains in a coastal plain region (Alt Empordà, Northern Spain); *J. Hydrol.* **409(1–2)** 407–422.

Zarroca M, Linares R, Rodellas V, Garcia-Orellana J, Roqué C, Bach J and Masqué P 2014 Delineating coastal groundwater discharge processes in a wetland area by means of electrical resistivity imaging, ^{224}Ra and ^{222}Rn; *Hydrol. Process.* **28(4)** 2382–2395.

Zektser I S, Everett L G and Dzhamalov R G 2006 Submarine Groundwater, CRC Press, 466p.

Corresponding editor: Subimal Ghosh